Advances in World Medical Research, 2026, 2(2), 40-63
https://doi.org/10.71204/pk2jdq31

GCN5-Catalyzed WSTF Benzoylation Activates Tumor Glycolysis

Yiwei Liu [1, #], Yunjie Pei [2, #], Shuqing Wang [3,4, *], Zhihao Shen[1, 5], Yaqi Wang [6], Yan Liu [1, 7, *]

[1] College of Life Science, North China University of Science and Technology, Tangshan 063210, China

[2] North China University of Science and Technology Affiliated Hospital, Tangshan 063000, China

[3] School of Public Health, North China University of Science and Technology, Tangshan 063210, China

[4] Hospital of North China University of Science and Technology, Tangshan 063210, China

[5] Department of Clinical Laboratory, North China University of Science and Technology Affiliated Tangshan Maternal and Child Health Hospital, Tangshan 063000, China

[6] Department of Breast Center, Breast Center of the Affiliated Hospital of North, China University of Science and Technology, Tangshan 063000, China

[7] Hebei Key Laboratory of Molecular Oncology, Tangshan People's Hospital, Tangshan 063000, China.

*** Correspondence:**

Shuqing Wang

wsq7992023@163.com

Yan Liu

liuysm@ncst.edu.cn

[#] Yiwei Liu and Yunjie Pei are co-first authors and contributed equally to this article.

Received: 30 April 2026/ Accepted: 25 May 2026/ Published online: 1 June 2026

Abstract

Williams syndrome transcription factor (WSTF), traditionally recognized as a nuclear-localized transcription factor and histone tyrosine kinase, has been detected in the cytoplasm of various cancer cells in our previous observations. This finding suggests the existence of an uncharacterized nucleocytoplasmic shuttling mechanism and extranuclear functions of WSTF. This study aims to investigate whether WSTF's subcellular localization is regulated by novel post-translational modifications, and to clarify its cytoplasmic functions and role in tumor metabolic reprogramming. Through post-translational modification proteomics analysis, we identified lysine benzoylation at position 181 (K181) of WSTF. After knocking down candidate enzyme genes individually with specific siRNAs, WB analysis revealed a significant decrease in

WSTF-K181 benzoylation levels only when GCN5 was knocked down, suggesting that GCN5 is a potential enzyme catalyzing this modification. Functional assays demonstrated that K181 benzoylation is a key driver for WSTF translocation from the nucleus to the cytoplasm. Furthermore, 4D-Labelfree tyrosine phosphorylation proteomics unexpectedly identified hexokinase 1 (HK1) as a novel cytoplasmic substrate of WSTF. In vitro and in vivo experiments verified that WSTF directly binds to HK1 and phosphorylates it at tyrosine 667, thereby enhancing HK1 kinase activity and promoting glucose uptake and lactate production. Functionally, expression of wild-type WSTF significantly promoted the proliferation, migration, and in vivo tumorigenicity of breast cancer cells, while the kinase-inactive mutant (C338A) or benzoylation-deficient mutant (K181A) remarkably attenuated these oncogenic effects of WSTF. This study is the first to reveal a novel mechanism by which GCN5-mediated benzoylation regulates WSTF nucleocytoplasmic shuttling. Additionally, we discovered that WSTF drives tumor glycolysis in a non-canonical manner by directly phosphorylating the metabolic enzyme HK1. Our findings break through the traditional understanding of WSTF functions and provide a new perspective for deciphering tumor metabolic reprogramming.

Keywords: WSTF; GCN5; Benzoylation; Cancer; Glycolysis

1. Introduction

Williams syndrome transcription factor (WSTF), also known as BAZ1B (bromodomain adjacent to the zinc finger domain 1B), is a novel tyrosine kinase encoded by the WBSCR9 gene, with no homology to other known kinase molecules (Sharif et al., 2021). First identified in patients with Williams syndrome in 1998 (Lu et al., 1998; Peoples et al., 1998), subsequent extensive studies have revealed its diverse functions, including involvement in metabolism, replication, transcription, DNA damage repair, and cell cycle regulation. These functions are all associated with the complex multisystem defects, multiple organ developmental disorders, intellectual and cognitive abnormalities characteristic of this syndrome (Barnett & Krebs, 2011; Sharif et al., 2021). In 2012, Ewa E. Henning et al. first reported six kinases with altered expression in a study analyzing colon cancer biomarkers, among which WSTF was included (Hennig et al., 2012). However, this report did not conduct an in-depth analysis of the mechanism by which WSTF exerts its effects. In 2016, our team demonstrated through three articles that, regulated by upstream Ras pathway signals, the phosphorylation level of serine 158 (S158p) in WSTF can modulate histone acetylation modifications (acetylation, ac) - H3K9ac and H4K16ac, thereby affecting chromatin structure and downstream gene expression, and ultimately regulating breast cancer development (Liu et al., 2016; Li et al., 2016; Wang e al., 2016). In 2020, we further reported that acetylation modification of lysine 426 (Lys, K) (K426ac) can promote WSTF activity and oncogenic functions (Liu et al., 2020). Although several subsequent studies have explored the relationship between WSTF and tumorigenesis, drug resistance, and signaling pathways based on our team's reports, all these analyses are grounded in the aforementioned Williams syndrome-related research (Zhang et al., 2012; Meng et al., 2016; Kang et al., 2022; Huang et al., 2022; Nargund et al., 2022).

Benzoylation is a newly discovered acylation modification, and currently the only known lysine acylation modification containing a benzene ring. Existing studies have shown that it can be induced by sodium benzoate (NaBz) through the generation of benzoyl-CoA. Sodium benzoate is a widely used food additive and an FDA-approved drug for the treatment of hyperammonemia caused by urea cycle disorders; benzoyl-CoA is also an intermediate in the degradation of numerous aromatic substrates in intestinal microbiota (Ren et al., 2021). Currently, the regulatory mechanisms and physiological/pathological functions of benzoylation remain unclear.

GCN5, also known as KAT2A (lysine acetyltransferase 2A), is highly expressed in various tumors such as breast cancer, colon cancer, and prostate cancer, and is closely associated with drug resistance, cell proliferation, migration, and epithelial-mesenchymal transition (Oh et al., 2020; Yuan et al., 2021).

In humans, GCN5 has been extensively studied for its roles in epigenetic regulation and pathogenic mechanisms of cancer (Chen et al., 2013; Yin et al., 2015; Liu et al., 2015; Majaz et al., 2016; Koutsogiannouli et al., 2017; Shao et al., 2018; Qiao et al., 2018; Kahl et al., 2019; Farria et al., 2020), diabetes, osteoporosis, systemic lupus erythematosus, malaria, myopathy, visual impairment, and other diseases (Lerin et al., 2006; Mao et al., 2009; Leung et al., 2015; Li et al., 2016; Kumar et al., 2017; Carrillo-Rosas et al., 2019; Addicks et al., 2022; Li et al., 2022).

Glycometabolism is an important pathway for tumor cells to obtain energy, and hexokinase (HK) is the enzyme that catalyzes the key step in glycolysis—the conversion of glucose (G) to glucose-6-phosphate (G-6-P) (Smith, 2000; Wilson, 2003; Hanahan et al., 2011; Kierans & Taylor, 2024). As a core biochemical process maintaining cellular energy supply and life activities in organisms, glycometabolism encompasses critical links such as glycolysis, tricarboxylic acid cycle, pentose phosphate pathway, and gluconeogenesis. It not only achieves ATP production and material transformation through multiple pathways but also acts as a signaling hub regulating cellular functions (Kierans & Taylor, 2024). Its spatiotemporal precise regulation relies on the coordinated action of key enzymes such as phosphofructokinase-1, and it plays a crucial role in tumor metabolic reprogramming (Li et al., 2025).

The cytoplasmic distribution of WSTF in various tumor cells challenges traditional cognition, but the key signal driving its nuclear export has long remained unknown. In recent years, lysine benzoylation has been identified as a novel acylation modification, whose physiological and pathological functions are unclear, and its association with tumor metabolism is completely unexplored. Based on this, we propose the scientific hypothesis: The nucleocytoplasmic shuttling of WSTF is precisely regulated by benzoylation, and cytoplasmic WSTF directly participates in tumor cell metabolic regulation by phosphorylating non-histone substrates. By integrating modification proteomics, biochemical, and cell biology approaches, this study validates this hypothesis and reveals a complete pathway from "modification signal" to "localization change", followed by "substrate recognition" and "functional output".

2. Methods

2.1. Cell Culture

SW620, MDA-MB-157, Hela cells were purchased from the Cell Bank of the Chinese Academy of Sciences (Beijing). HEK293T, and Ada2$^{-/-}$ HEK293 cells were purchased from Saier Biolabs (Tianjin). Each cell line was cultured in an appropriate growth medium in accordance with the recommendations of the respective suppliers (Cell Resource Center, Institute of Basic Medical Sciences, or Chinese Academy of Medical Sciences). Cell lines were routinely tested using short tandem repeat profiling method, and mycoplasma infection was tested monthly.

2.2. Plasmid Construction

The construction process of expression plasmids for wild-type (WT) and three mutant-type (K181A, K181R, C338A) WSTF (Williams Syndrome Transcription Factor), GCN5 (General Control Nonderepressible 5) and hexokinase 1 (HK1) was as follows: First, site-directed mutagenesis was used, with the wild-type cDNA of each target gene (WSTF, GCN5, HK1) as the template, and specific primers were designed to introduce the target mutation sites (K181A means that the lysine at position 181 of WSTF protein was mutated to alanine, K181R means that the lysine at position 181 was mutated to arginine, and C338A means that the cysteine at position 338 was mutated to alanine), to amplify DNA fragments containing wild-type or mutant-type target genes. Subsequently, these amplified target gene fragments were cloned into the corresponding eukaryotic expression vectors respectively. The vectors used included pCDNA3.1 vectors with Flag tag, HA tag or Myc tag. Finally, recombinant expression plasmids capable of expressing wild-type and mutant-type WSTF, GCN5 and HK1 proteins with different tags were constructed.

2.3. Antibodies and Reagents

Site-specific modification antibodies: anti-WSTF-K181bz and anti-p-Y667-HK1 were custom-synthesized by PTM Bio Company. Anti-WSTF (#ab51256), anti-GCN5 (#ab217876), and anti-Ada2 (#ab164942) were purchased from Abcam. Anti-HK1 (#ET1609-28), anti-Tubulin (#HA721913), anti-GAPDH (#ET1601-4), anti-H3 (#M1309-1), anti-β-actin (#EM21002), and anti-AIF (#ET1603-4) were obtained from HUABIO. The Hexokinase Activity Assay Kit, 2-NBDG, Lactate Assay Kit, CCK-8 reagent, and Subcellular Fractionation Kit were purchased from Tianjin Sai'er Biotechnology Co., Ltd.

2.4. Western Blotting

Cells used for immunoprecipitation (IP) and western blotting (WB) were collected, resuspended in RIPA lysis buffer (#P0013B; Beyotime Biotechnology), subjected to 15 ultrasound pulses (each exposure lasting 1 s), and centrifuged at 15,000g at 4°C for 30 min. For IP of target proteins, the supernatant was incubated with the appropriate antibody and protein A/G agarose beads (Santa Cruz Biotechnology, Inc.). For WB, either total cell lysates or immunoprecipitates were boiled and proteins separated using a 10% sodium dodecyl sulfate-polyacrylamide gel electrophoresis (SDS-PAGE) system. The target proteins were transferred onto a polyvinylidene fluoride membrane (Roche), sealed in a 5% skim milk solution for 1 h, then hybridized with the corresponding antibodies. Protein signaling was enhanced using

chemiluminescent horseradish peroxidase-conjugated antibodies. Images were analyzed using an SH-Compact 523 chemiluminescence imaging system (Hangzhou Shenhua Technology Co., Ltd.).

2.5. GST Pull-Down

Escherichia coli strain BL21 was transformed with protein expression plasmids and subsequently induced with 0.2mM isopropyl-β-D-thiogalactoside at 20°C. Labeled proteins were purified using Ni-NTA beads or GST Sepharose beads (GE). For GST pull-down tests, protein mixtures were incubated with GST pull-down buffer for 2h at 4°C, followed by pull-down assay. The precipitates underwent a washing and separation process using SDS-PAGE, followed by staining of proteins with Coomassie brilliant blue. WB with specific antibodies was used to detect target proteins in the precipitant.

2.6. Immunofluorescence Assay

Cells were cultured on glass coverslips in 6-well plates until reaching 50% confluence. The cells were fixed with 100% cold methanol on ice for 10 minutes, then permeabilized with 0.2% Triton X-100 in phosphate-buffered saline (PBS) at room temperature for 10 minutes. The coverslips were first washed twice with washing buffer (0.02% Triton X-100, 1.5% BSA, and 1 mM NaN_3), then blocked in blocking buffer (5% BSA, 0.02% Triton X-100, and 1 mM NaN_3) for 1 hour, followed by incubation with primary antibodies for 1 hour. Next, the cells were rinsed four times with washing buffer (5 minutes each time) and incubated with appropriate secondary antibodies in blocking solution at 37 °C for 1 hour in a dark box. Finally, after nuclear staining and fixation, the samples were observed under a microscope.

2.7. Dot blot

For the Dot blot assay, gradient concentrations (1μg, 0.5μg) of WT and K181bz-modified WSTF peptide samples were prepared, alongside a 0 μg blank control. A nitrocellulose (NC) membrane was pre-equilibrated in TBST buffer; samples of each concentration were then spotted onto the membrane in a predefined array (2 μL per spot) using a micropipette, followed by air-drying at room temperature for 15 min to ensure complete peptide immobilization. Subsequently, the membrane was submerged in TBST blocking buffer supplemented with 5% non-fat dry milk and incubated for 1 h on a rotating shaker at room temperature to block non-specific binding sites. After removing the blocking buffer, the membrane was incubated separately with the anti-K181bz primary antibody (diluted to the recommended working concentration) or a biotin affinity detection reagent overnight on a rotating shaker at 4°C. On the following day, unbound reagents were removed by washing the membrane three times (10 min per wash) with TBST buffer. Finally, chemiluminescent substrate was applied, and signals were acquired using a chemiluminescence imaging system.

2.8. Benzoyltransferase Activity Assay

The reaction mixture was prepared in vitro with 50 mM Tris-HCl, 1 mM DTT (pH 7.5), 3.2 mM $MgCl_2$, 40 mM NaCl, 0.1 mM EDTA, 2 μM histone octamer, and 5 μM Ada2-Gcn5. After incubation at 30 °C for 5 minutes, 200 μM benzoyl-CoA was added to initiate the reaction. The

reaction was terminated at the desired time points by adding 0.5% trifluoroacetate. The level of benzoylation modification was detected by Western blot using specific antibodies.

2.9. Co-immunoprecipitation

Total cellular proteins were extracted by lysing target cells on ice with RIPA lysis buffer supplemented with protease inhibitors and phosphatase inhibitors. A portion of the protein sample was reserved as the Input control. For the remaining protein sample, specific primary antibodies (e.g., Anti-WSTF, Anti-Flag, Anti-HA antibodies) were added, followed by gentle oscillation and incubation at 4°C overnight. Subsequently, Protein A/G agarose beads were added for an additional 4-hour incubation to capture immune complexes. After multiple washes with RIPA lysis buffer, SDS loading buffer was added, and the samples were denatured by boiling in a water bath. The expression of target binding proteins in the immune complexes was detected by Western blot.

2.10. Transcriptomics Analysis

At least 3 biological replicates were set up for each group. Total RNA was extracted from cells/tissues using TRIzol reagent (Invitrogen). RNA purity (A260/A280 ratio: 1.8~2.0; A260/A230 ratio ≥ 2.0) and integrity (RNA Integrity Number, RIN ≥ 7.0) were verified using a Nanodrop 2000 spectrophotometer and an Agilent 2100 Bioanalyzer, respectively. One microgram of qualified RNA was used to construct sequencing libraries with the VAHTS® mRNA-seq V2 Library Prep Kit. Subsequent quality control of library insert size and concentration was performed using an Agilent 2100 Bioanalyzer and a Qubit fluorometer. Libraries were sequenced on an Illumina sequencing platform. Raw data were filtered and aligned to the reference genome. Differentially expressed genes (DEGs) were screened using DESeq2 software with the criteria of $|\log_2 (\text{fold change})| \geq 1$ and $P < 0.05$.

2.11. HK Activity Assay

Briefly, cells that were cultivated in 60-mm petri dishes were collected and placed in 400μL lysis buffer (50mM potassium dihydrogen phosphate, 2mM ethylenediaminetetraacetic acid (EDTA), 2mM dithiothreitol, 20mM sodium fluoride [Na F]). Homogenates were then prepared at 4°C and centrifuged at 18,000g at 4°C for 15min. A 40-μL aliquot of the supernatant was introduced into a 1-mL volume of the following reaction buffer: 100mM Tris-HCl at pH 8.0, 10mM ATP, 0.5mM EDTA, 10mM $MgCl_2$, 2mM glucose, 0.2mM $NADP^+$, and 30μg of glutathione (GST)-glucose-6-phosphate dehydrogenase (G6PD) purified from Escherichia coli. HK activity was identified by measuring the conversion of NADP to NADPH using spectrophotometry at a wavelength of 340nm and a temperature of 37°C. This conversion is dependent on the presence of GST and G6PD. The observed increase in optical density, determined at 2min over a total of 15 cycles, was found to be associated with an elevated concentration of NADPH. Total HK activity was determined by analyzing the logarithmic stage of the resulting curve and calculating its slope. HK activity in various samples within the same investigation was standardized by normalization to the protein content of the respective lysates.

2.12. Glucose Uptake Assay

The cell lines were inoculated in six-well culture plates, and cultured in complete growth medium for 24 h, low-glucose medium (Hyclone) for 4 h, and glucose-free medium for 30 min in sequence. Subsequently, the cells in each well were treated with a solution containing 0.25μCi 2-[1,2-^{3}H]- deoxy glucose (2-DG, Perkin Elmer). After 10 min, the cells were washed three times with phosphate-buffered saline (PBS), and then lysed with 0.2 M sodium hydroxide (NaOH). The concentration of 2-DG in the cell lysate was determined by liquid scintillation counting

2.13. Lactate Production Assay

Cellular lactate production under normoxia was measured using a lactic acid assay kit (A019-2-1; NanJing JianCheng Bioengineering Institute). Briefly, the cells were introduced into six-well plates and cultivated in medium for 24h, after which fresh medium was supplied for another 4h of incubation, followed by determination of the lactic acid content in the culture medium.

2.14. Cell proliferation assay

Cell proliferation was assessed by direct cell counting. Briefly, cells stably expressing Vector, WT-WSTF, or mutant WSTF constructs were seeded in 6-well plates at a density of 2×10^4 cells per well. On days 1, 2, 3, 4, and 5 after seeding, cells were harvested by trypsinization, resuspended in PBS, and counted using a hemocytometer. The number of viable cells was recorded, and cell growth curves were plotted based on the mean cell counts from three independent experiments.

2.15. Xenograft mouse model

Tumor cells (5×10^6 cells per mouse) stably expressing Vector, WT-WSTF, C338A-WSTF, or K181A-WSTF were subcutaneously injected into the right flank of 6-week-old male BALB/c nude mice (n=5 per group). After visible tumor nodules (≥2 mm in diameter) formed (typically 7 days post-inoculation), tumor growth was monitored every 3 days by measuring tumor length (L) and width (W) with calipers; tumor volume was calculated using the formula: $V = 0.5 \times L \times W^2$. At the experimental endpoint (21 days post-inoculation), mice were euthanized, and tumors were dissected and weighed to obtain relative tumor weight (normalized to the Vector group).

2.16. Proteomics Analysis

Standard mass spectrometry techniques were used to perform 4D label-free tyrosine phosphorylation proteomics analysis and post-translational modification (PTM) proteomics analysis to screen for differentially modified proteins and identify modification sites.

2.17. Statistical Analysis

Experimental data are presented as mean ± standard error of the mean (mean ± SEM). Statistical analysis was performed using GraphPad Prism software. Comparisons between groups were conducted using Student's t-test or one-way analysis of variance (one-way ANOVA). AP value < 0.05 was considered statistically significant.

3. Result

3.1. WSTF Localizes to the Cytoplasm in Multiple Cancer Cells and Is Regulated by Benzoylation Modification

We first examined the subcellular distribution of WSTF in cancer cells. Using subcellular fractionation and Western blot analysis in SW620 colon cancer cells (Figure 1A), we found that WSTF predominantly localizes to the cytoplasm, with weaker signals also detected in the nucleus.

To investigate the regulatory mechanism underlying this nucleocytoplasmic distribution, we profiled post-translational modifications (PTMs) of WSTF. Immunoprecipitation with a pan-benzoylation antibody followed by liquid chromatography-tandem mass spectrometry (LC-MS/MS) identified a previously unreported benzoylation modification at lysine 181 (K181) of WSTF. Sequence alignment revealed that this residue is highly evolutionarily conserved across vertebrate species (Figure 1B).

We then validated the specificity of a custom-made anti-K181-benzoylation antibody using dot blot assays, which confirmed its specific recognition of the benzoylated WSTF peptide, with no cross-reactivity against the unmodified wild-type peptide (Figure 1C).

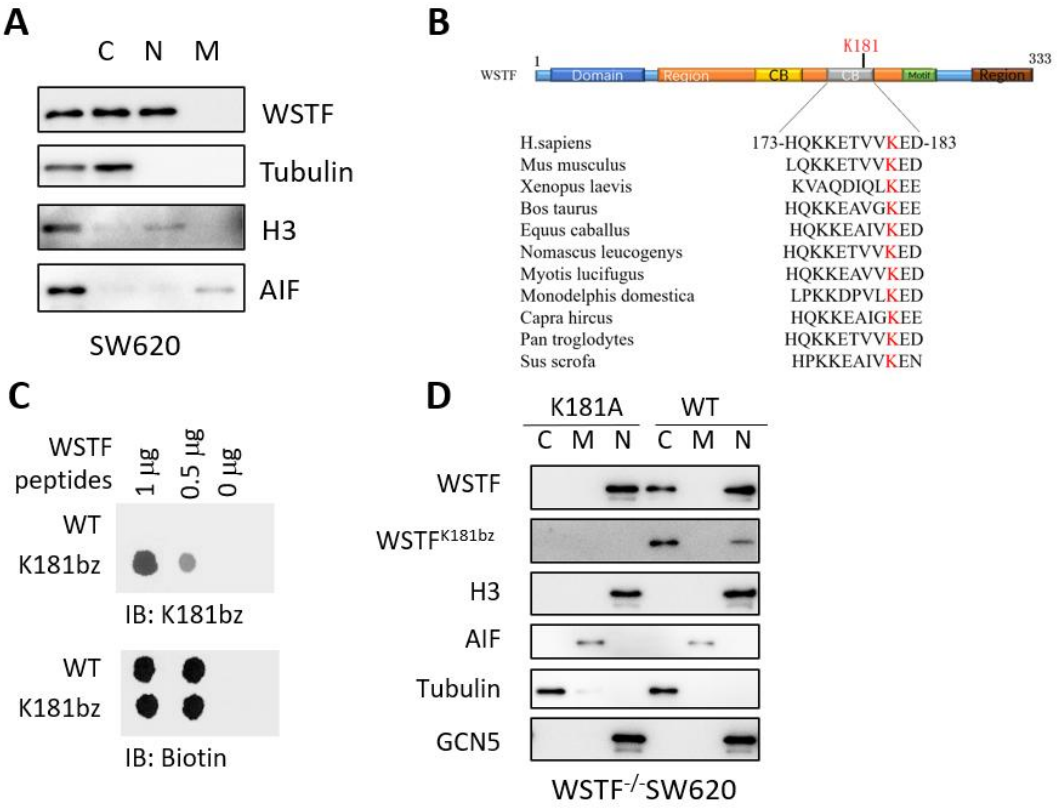

Figure 1. WSTF localization and K181 benzoylation in cancer cells

Note: A. Subcellular fractionation and Western blot analysis showing the distribution of endogenous WSTF in SW620 colon cancer cells. C, cytoplasm; N, nucleus; M, membrane. Tubulin, histone H3, and AIF were used as purity markers for the cytoplasmic, nuclear, and membrane fractions, respectively.

B. Schematic illustration of WSTF domains and multiple-sequence alignment showing evolutionary conservation of the K181 residue across vertebrate species.

C. Dot blot assay validating the specificity of the custom-made anti-WSTF K181bz antibody using biotin-labeled WT and K181bz-modified WSTF peptides.

D. Subcellular fractionation and Western blot analysis of WSTF localization in $WSTF^{-/-}$ SW620 cells rescued with wild-type (WT) or K181A-mutant WSTF.

To test whether K181 benzoylation regulates WSTF localization, we reconstituted WSTF-knockout SW620 cells with either wild-type (WT) WSTF or the benzoylation-deficient K181A mutant. Subcellular fractionation and Western blot analysis showed that, compared to WT WSTF, the K181A mutant exhibited significantly reduced cytoplasmic enrichment and a marked increase in nuclear localization (Figure 1D). Notably, the WSTF-K181bz signal was detected predominantly in the nuclear fraction in the WT rescue group, but was undetectable in the K181A mutant group. Together, these results indicate that K181 benzoylation is a critical modification that promotes the cytoplasmic translocation of WSTF in cancer cells.

3.2. Transcriptome Analysis Reveals the Functional Impact of WSTF Benzoylation Modification

To investigate the functional consequences of WSTF benzoylation, we established stable cell models in SW620 cells: WSTF-knockout cells were stably transfected with either the benzoylation-deficient WSTF-K181A plasmid or the wild-type WSTF-WT plasmid. The resulting cell lines, hereafter referred to as the K181A-WSTF group (experimental group) and the WT-WSTF group (control group), were subjected to RNA sequencing (RNA-seq) for transcriptome analysis.

Using the cutoff criteria of $p < 0.05$ and $|\log_2 \text{fold change (FC)}| > 0.58$, a total of 112 differentially expressed genes (DEGs) were identified in the K181A-WSTF vs. WT-WSTF comparison, including 53 upregulated and 59 downregulated genes (Figure 2A). A volcano plot visualized the global gene expression changes, where red dots represent upregulated DEGs, green dots denote downregulated DEGs, and gray dots indicate genes with no significant difference (Figure 2B). The hierarchical clustering heatmap showed distinct expression patterns of DEGs between the two groups, with red indicating high expression and blue indicating low expression (Figure 2C). Gene Ontology (GO) analysis annotated the functions of the DEGs. GO classification (Figure 2D) showed that most DEGs belonged to Biological Process (BP), followed by Molecular Function (MF) and Cellular Component (CC). BP terms were enriched in biological adhesion, cellular process, and biological regulation; CC terms were mainly related to extracellular matrix, membrane structures, and macromolecular complexes; MF terms were dominated by catalytic and binding activities.

GO enrichment of the top 30 terms (Figure 3A) further showed that BP terms were highly enriched in cell proliferation regulation, mitotic cycle, and osteoblast differentiation; CC terms were concentrated in extracellular matrix, membrane raft, and exosomes; MF terms were mainly associated with receptor ligand binding, enzyme regulation, and oxidoreductase activity. These results suggest that DEGs are involved in cellular physiological processes, extracellular matrix organization, and molecular interactions.

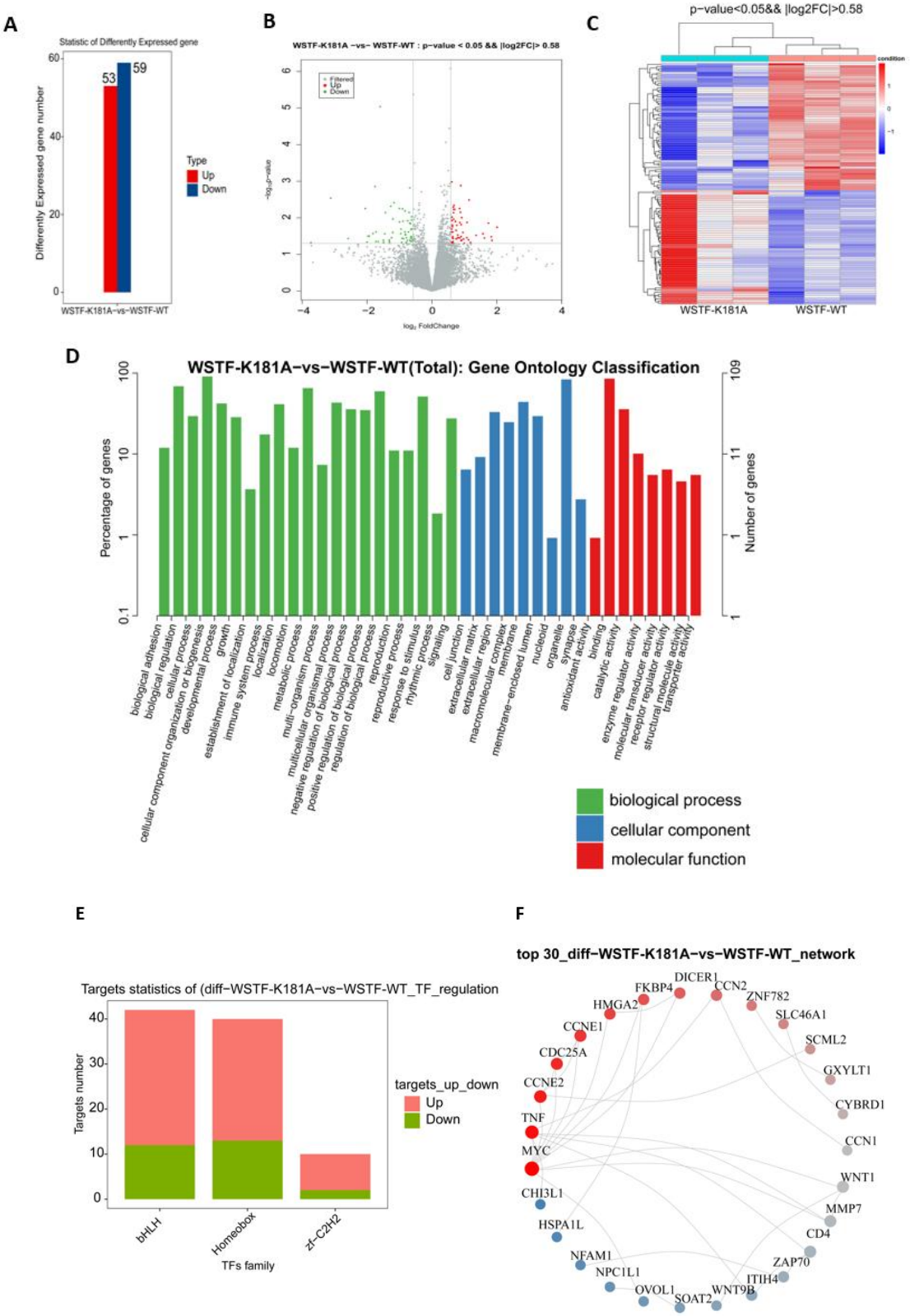
A
Statistic of Differently Expressed gene
Differently Expressed gene number
53
59
Type
Up
Down
WSTF-K181A−vs−WSTF-WT
B
WSTF-K181A −vs− WSTF-WT : p−value < 0.05 && |log2FC|> 0.58
Filtered
Up
Down
C
p−value<0.05&& |log2FC|>0.58
condition
WSTF-K181A
WSTF-WT
D
WSTF-K181A−vs−WSTF-WT(Total): Gene Ontology Classification
Percentage of genes
Number of genes
biological adhesion
biological regulation
cellular process
cellular component organization or biogenesis
developmental process
growth
establishment of localization
immune system process
localization
locomotion
metabolic process
multi−organism process
multicellular organismal process
negative regulation of biological process
positive regulation of biological process
regulation of biological process
reproduction
reproductive process
response to stimulus
rhythmic process
signaling
cell junction
extracellular matrix
extracellular region
macromolecular complex
membrane
membrane−enclosed lumen
nucleoid
organelle
synapse
antioxidant activity
binding
catalytic activity
enzyme regulator activity
molecular transducer activity
receptor regulator activity
structural molecule activity
transporter activity
biological process
cellular component
molecular function
E
Targets statistics of (diff−WSTF-K181A−vs−WSTF-WT_TF_regulation
Targets number
targets_up_down
Up
Down
bHLH
Homeobox
zf−C2H2
TFs family
F
top 30_diff−WSTF-K181A−vs−WSTF-WT_network
DICER1
FKBP4
CCN2
ZNF782
HMGA2
SLC46A1
CCNE1
SCML2
CDC25A
GXYLT1
CCNE2
CYBRD1
TNF
CCN1
MYC
WNT1
CHI3L1
MMP7
HSPA1L
CD4
NFAM1
ZAP70
NPC1L1
ITIH4
OVOL1
WNT9B
SOAT2

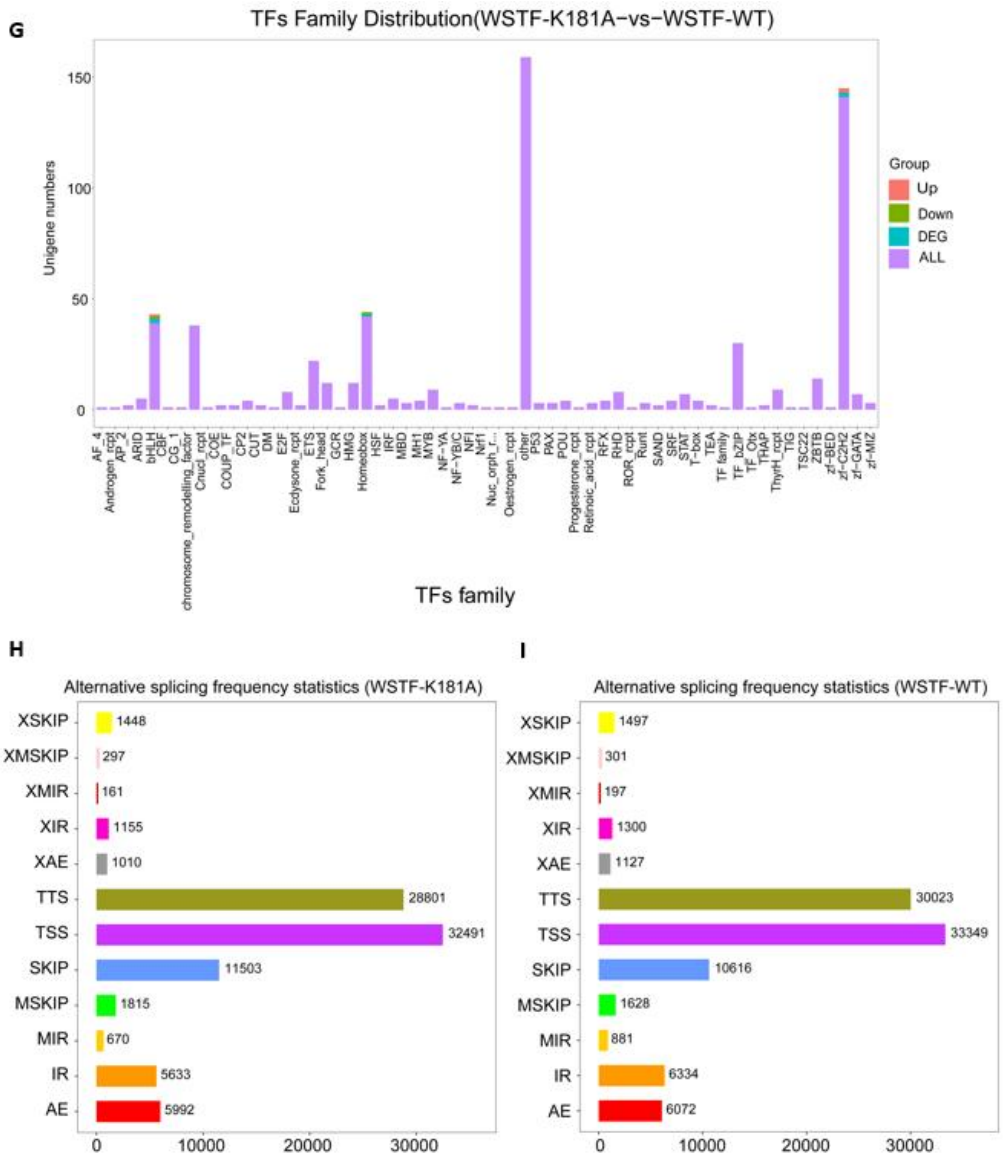

Figure 2. Transcriptomic analysis of the comparison between K181A-mutant WSTF and wild-type WSTF

Notes: A. Quantitative statistics of differentially expressed genes (DEGs). Blue bars represent downregulated genes, and red bars represent upregulated genes. The graph shows the distribution of the number of genes with significant differences ($P<0.05$ and $|logFC|>1$) between two sample groups (e.g., control group vs. experimental group).

B. Volcano plot showing the differential expression results. Gray dots represent genes with no significant difference, while red and green dots represent genes with significant differences.

C. In the graph, red indicates relatively highly expressed protein-coding genes, and blue indicates relatively lowly expressed protein-coding genes.

D. Gene Ontology (GO) enrichment analysis of DEGs. The x-axis represents the names of GO terms.

E. Target gene statistics of differential WSTF (K181A vs WT) in TF regulation. The bar chart displays the number of target genes corresponding to different transcription factor (TF) families (bHLH, Homeobox, zf-C2H2). Red represents upregulated target genes, and green represents downregulated target genes.

F. TF family distribution of differential WSTF (K181A vs WT). The X-axis denotes TF families, and the Y-axis denotes gene counts. Purple represents all genes regulated by the corresponding TF family; blue represents differential TFs regulated by the family; red/green represent upregulated/downregulated differential TFs, respectively.

G. Top 30 target gene interaction network of differential WSTF (K181A vs WT). Nodes represent genes, and edges represent interaction relationships. Red nodes indicate upregulated differentially expressed genes (DEGs), while blue nodes indicate downregulated DEGs. Node size is positively correlated with the number of associated genes.

H-I. Frequency statistics of alternative splicing events in WSTF-K181A vs WSTF-WT. The left panel corresponds to the WSTF-K181A group, and the right panel corresponds to the WSTF-WT group. The X-axis represents alternative splicing types (e.g., XSKIP, XIR), and the Y-axis represents event frequency; different colors correspond to distinct splicing types.

Kyoto Encyclopedia of Genes and Genomes (KEGG) pathway enrichment analysis of the top 20 pathways (Figure 3B) showed significant enrichment in cancer-related pathways (e.g., gastric cancer and small cell lung cancer pathways), viral infection pathways (e.g., Epstein-Barr virus and human papillomavirus infection pathways), and cellular signaling pathways (e.g., Hippo and TGF-β signaling pathways). Notably, cancer-related pathways exhibited the highest enrichment score, with additional enrichment of cell cycle and cellular senescence pathways, implying that DEGs may contribute to tumorigenesis, cellular dysfunction, and the regulation of cell proliferation and homeostasis.

Transcription factor (TF) analysis indicated that the bHLH and Homeobox families are the core regulatory TFs mediating DEG upregulation in the K181A-WSTF vs. WT-WSTF comparison, while the New TF family covers the largest number of DEGs in this system, collectively regulating the differential gene expression between the two groups (Figure 2E-F). Protein-protein interaction (PPI) network analysis of the top 30 DEGs identified TYC and TNT as key regulatory hubs that interact with multiple genes. Blue nodes (e.g., ANPEC3) and gray nodes (e.g., ZNF99) represent interacting genes of different functional types, which participate in biological function regulation through multi-node interactions (Figure 2G).

Statistics of alternative splicing events showed that transcription start site (TSS) and transcription termination site (TTS) alternative splicing events were the most abundant in both the K181A-WSTF and WT-WSTF groups. Additionally, exon skipping (XSKIP) and intron retention (XMIR) events were also detected, though they were relatively rare. Furthermore, the frequency of each alternative splicing type differed between the two groups, suggesting that differential alternative splicing patterns may be involved in regulating the phenotypic differences（Figure 2H-I).

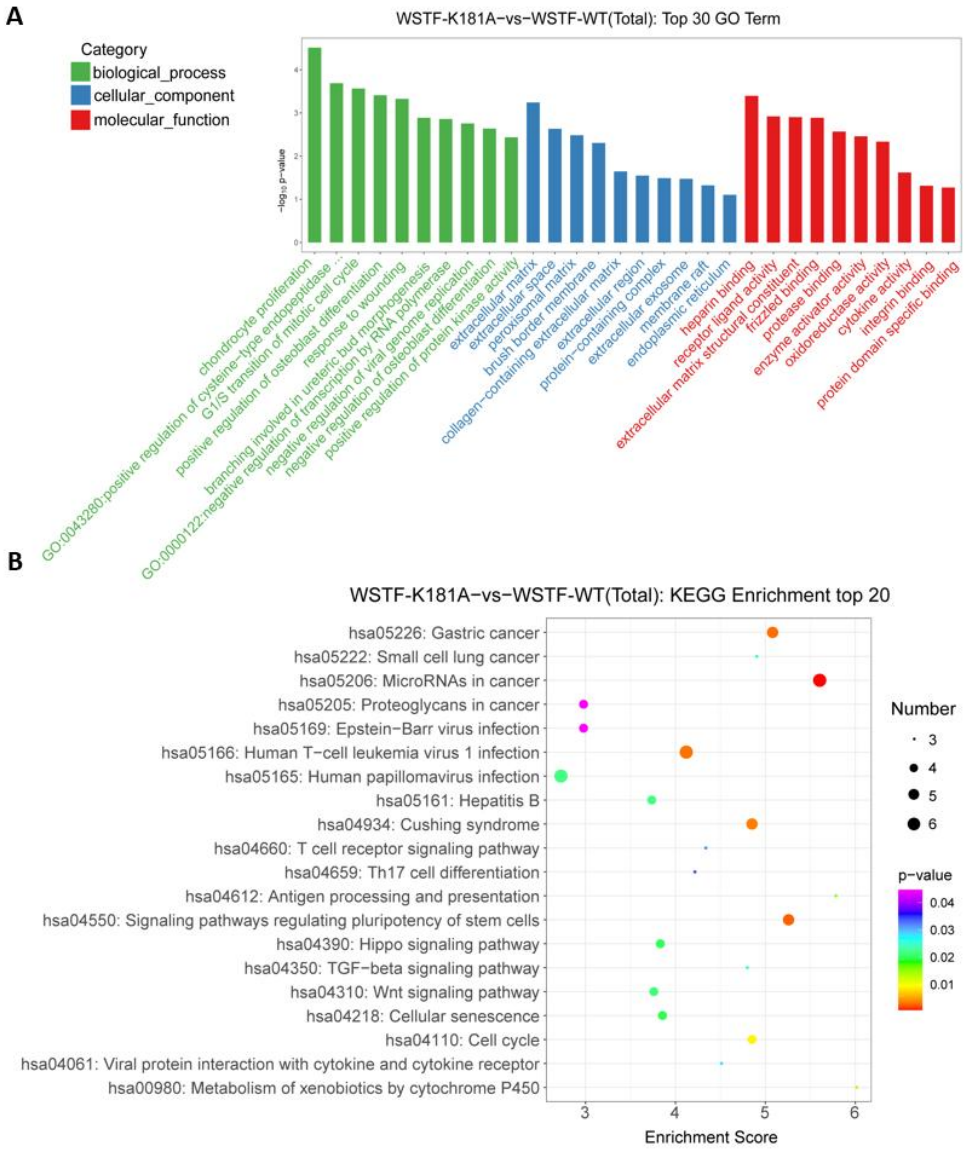

Figure 3. Functional enrichment analyses of differentially expressed genes between WSTF-K181A and WSTF-WT cells.

Note: A. Bar plot of the top 30 GO term enrichments. This plot displays the top 30 enriched terms from the Gene Ontology (GO) database for the differential group, with "-$\log_{10}$(P-value)" indicating enrichment significance. Different colors correspond to three GO categories: green (biological process), blue (cellular component), and red (molecular function).

B. Bubble plot of the top 20 KEGG pathway enrichments. This plot shows the top 20 enriched pathways from the KEGG database for the differential group. The bubble size represents the number of genes enriched in the pathway; the color corresponds to the P-value (more purple indicates a larger P-value, while more orange indicates a smaller P-value); the x-axis "Enrichment Score" denotes the enrichment score.

3.3. GCN5 is the Catalytic Enzyme for WSTF K181 Benzoylation

Based on previous reports suggesting that the acetyltransferases p300/CBP and GCN5/PCAF may catalyze protein benzoylation (Wilson, 2003; Kierans & Taylor, 2024; Li et al., 2025), we selected them as candidate enzymes. Following individual siRNA-mediated knockdown, Western blot analysis of WSTF K181 benzoylation showed that the modification level was significantly

reduced only in GCN5-knockdown cells, indicating that GCN5 is the primary candidate enzyme responsible for this modification.

Consistent with this result, GCN5 knockdown in MDA-MB-157 cells further decreased endogenous WSTF K181 benzoylation (Figure 4A); conversely, overexpression of Flag-tagged GCN5 markedly enhanced this modification (Figure 4B). Co-immunoprecipitation (Co-IP) assays confirmed that GCN5 interacts with both WSTF and Ada2, a core component of the GCN5-containing SAGA complex, in MDA-MB-157 cells (Figure 4C). A direct interaction between recombinant GCN5 and WSTF was further validated in vitro by GST pull-down assay (Figure 4D). Notably, the WSTF-K181R mutant exhibited attenuated binding affinity to GCN5 (Figure 4E), suggesting that the K181 residue itself is critical for the stable interaction between WSTF and GCN5.

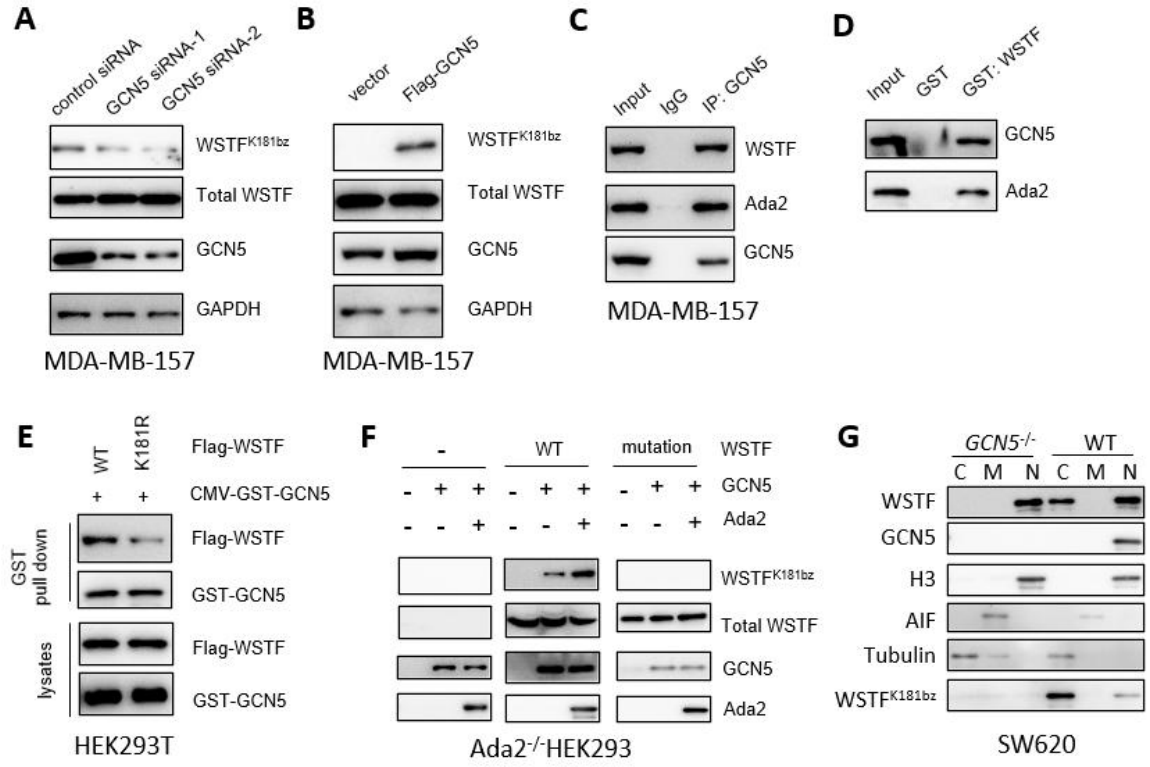

Figure 4. GCN5 is the modifying enzyme catalyzing WSTF K181 benzoylation

Note: A-B. Western blot analysis of WSTF benzoylation in MDA-MB-157 cells following GCN5 knockdown (A) or overexpression (B).

C. Co-IP assay showing endogenous interaction between WSTF and GCN5 in MDA-MB-157 cells.

D-E. GST pull-down assays demonstrating direct interaction between GCN5 and WSTF, with reduced binding to the K181R mutant (E).

F. In vitro benzoylation assay confirming that GCN5/Ada2 complex benzoylates WSTF at K181.

G. Subcellular localization of WSTF in wild-type and GCN5-knockout SW620 cells.

To confirm that GCN5 directly catalyzes WSTF benzoylation, we performed an in vitro reconstitution assay using Ada2-deficient HEK293 cells. Purified GCN5 alone was insufficient to modify WSTF, but the addition of Ada2 significantly enhanced GCN5-mediated benzoylation at

K181. In contrast, the K181-mutated WSTF failed to be modified under the same conditions (Figure 4F), demonstrating that the GCN5-Ada2 complex is the essential catalytic unit for WSTF K181 benzoylation.

To link this modification to WSTF localization, we examined the effect of GCN5 depletion on WSTF subcellular distribution in SW620 cells. GCN5 knockout significantly reduced WSTF cytoplasmic accumulation, while the nuclear pool of WSTF was increased (Figure 4G). Subsequent analysis across multiple tumor cell lines revealed that tumor cells with high GCN5 expression showed increased cytoplasmic accumulation of WSTF (Figure 5A).

3.4. WSTF Directly Binds to and Phosphorylates Hexokinase 1 (HK1)

To explore the cytoplasmic function of WSTF, we performed 4D-label-free tyrosine phosphoproteomics to identify its non-histone substrates (Supplementary Table 1). The results revealed that hexokinase 1 (HK1), a key rate-limiting enzyme in the glycolytic pathway, is a potential substrate of WSTF.

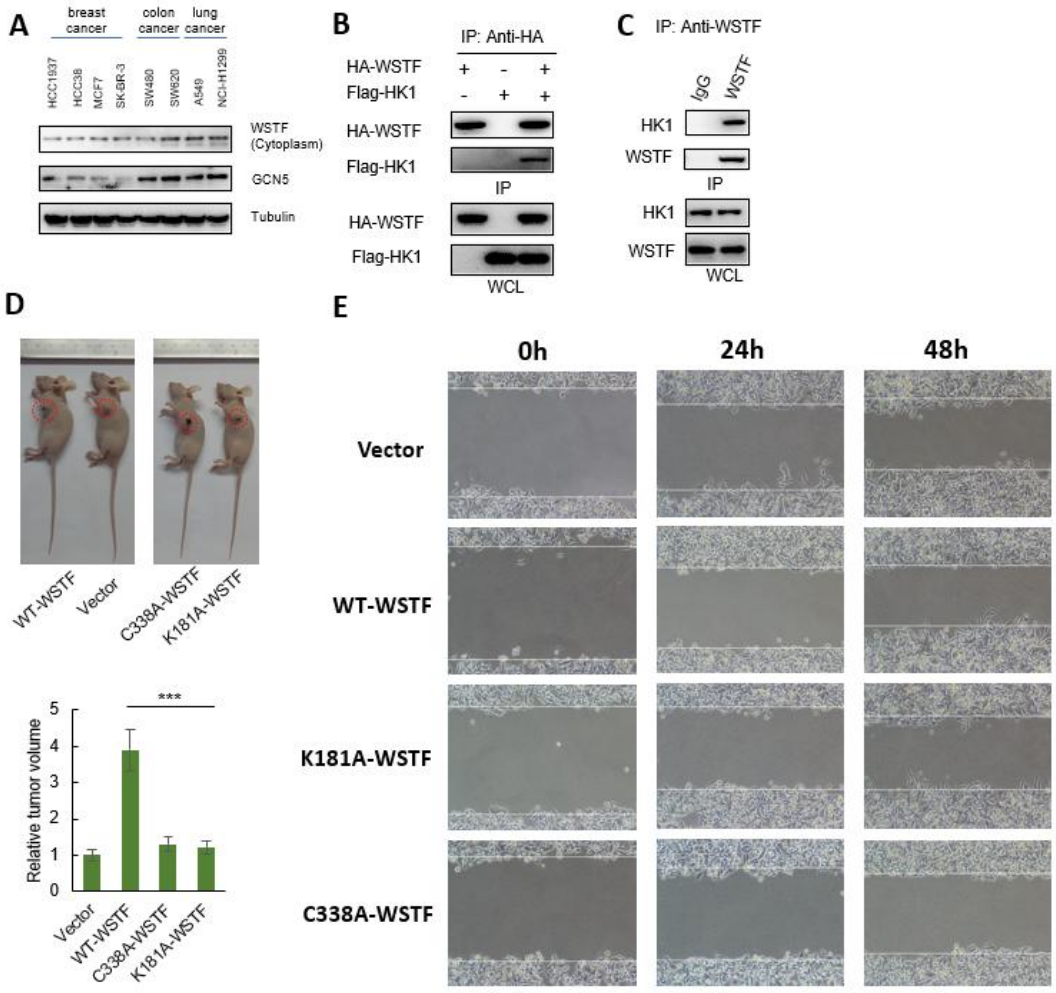

Figure 5. WSTF interacts with HK1 and GCN5; its benzoylation (K181) and acetylation (C338) regulate its cytoplasmic localization and/or protein complex formation.

Notes: A. Cellular proteins were extracted, and the correlation between GCN5 and WSTF localization was analyzed by Western blot.

B-C. Interaction between WSTF and HK1. GST pull-down and Co-immunoprecipitation (Co-IP) assays were performed to detect endogenous and exogenous interactions between WSTF and HK1 in vitro or in SW620 cells. WCL: Whole cell lysate.

D. SW620 cells transfected with the empty vector (Vector), wild-type WSTF (WT-WSTF), kinase-inactive mutant C338A-WSTF, or benzoylation-deficient mutant K181A-WSTF were subcutaneously implanted into nude mice. “Top panels” show representative images of the nude mice and subcutaneous tumors in each group (tumor sites are marked with red circles); “bottom panel” presents the relative quantitative statistics of tumor volumes across groups (data are expressed as the mean, with error bars representing standard deviation; ***P < 0.001 vs. the WT-WSTF group).

E. Wound healing assay of tumor cells. SW620 cells transfected with different plasmids were imaged at 0 h, 24 h, and 48 h post-wounding to demonstrate wound closure mediated by cell migration.

Co-immunoprecipitation (Co-IP) and GST pull-down assays confirmed the direct interaction between WSTF and HK1 both in vivo and in vitro (Figures 6A and 6B). Co-immunoprecipitation (Co-IP) assays confirmed the interaction between WSTF and HK1. Exogenously expressed HA-WSTF pulled down Flag-HK1 in co-transfected cells (Figure 5B). Endogenous Co-IP with anti-WSTF antibody further validated this interaction, using IgG as a negative control (Figure 5C).

Using a custom site-specific antibody against phosphorylated HK1-Y667, we verified that WSTF phosphorylates HK1 at the tyrosine 667 (Y667) residue. Co-expression of WSTF with HK1, but not the HK1-Y667F mutant, robustly induced HK1-Y667 phosphorylation (Figures 6C and 6D).

3.5. WSTF Enhances HK1 Activity and Promotes Glycolysis via Phosphorylating HK1 Y667

Next, we investigated the functional consequences of HK1-Y667 phosphorylation. Compared with wild-type HK1, the HK1-Y667F mutant showed significantly reduced enzymatic activity, and co-expression of kinase-dead WSTF failed to enhance HK1 activity (Figure 6E). An in vitro kinase assay further demonstrated that recombinant WSTF directly phosphorylates HK1 at Y667, which markedly enhanced the activity of wild-type HK1 but had no effect on the HK1-Y667F mutant (Figure 6F).

Consistent with these findings, in HeLa cells, WSTF significantly promoted glucose uptake and lactate production in an HK1-Y667 phosphorylation-dependent manner (Figures 6G and 6H), indicating that WSTF accelerates glycolytic flux through this mechanism.

3.6. WSTF Benzoylation and Kinase Activity Are Essential for Its Oncogenic Function

Finally, we evaluated the biological significance of this pathway at both the cellular and animal levels. In a SW620 cell xenograft model, overexpression of wild-type (WT) WSTF strongly promoted tumor growth, whereas the kinase-dead mutant (C338A) or the benzoylation-deficient mutant (K181A) significantly abrogated this oncogenic effect (Figure 6I and Figure 5D).

Consistent with the in vivo results, in vitro functional assays showed that the K181A and C338A mutants were significantly less potent than WT WSTF in promoting cell proliferation, migration, and lactate production (Figures 6J, 6K, 6L and Figure 5E). Specifically, wild-type WSTF significantly promoted the proliferation, migration, and lactate production of SW620 cells,

while WSTF with benzoylation deficiency (K181A) or kinase activity deficiency (C338A) completely lost these pro-tumorigenic functions.

Collectively, these findings demonstrate that the oncogenic function of WSTF depends on both its kinase activity and benzoylation-mediated nucleocytoplasmic shuttling.

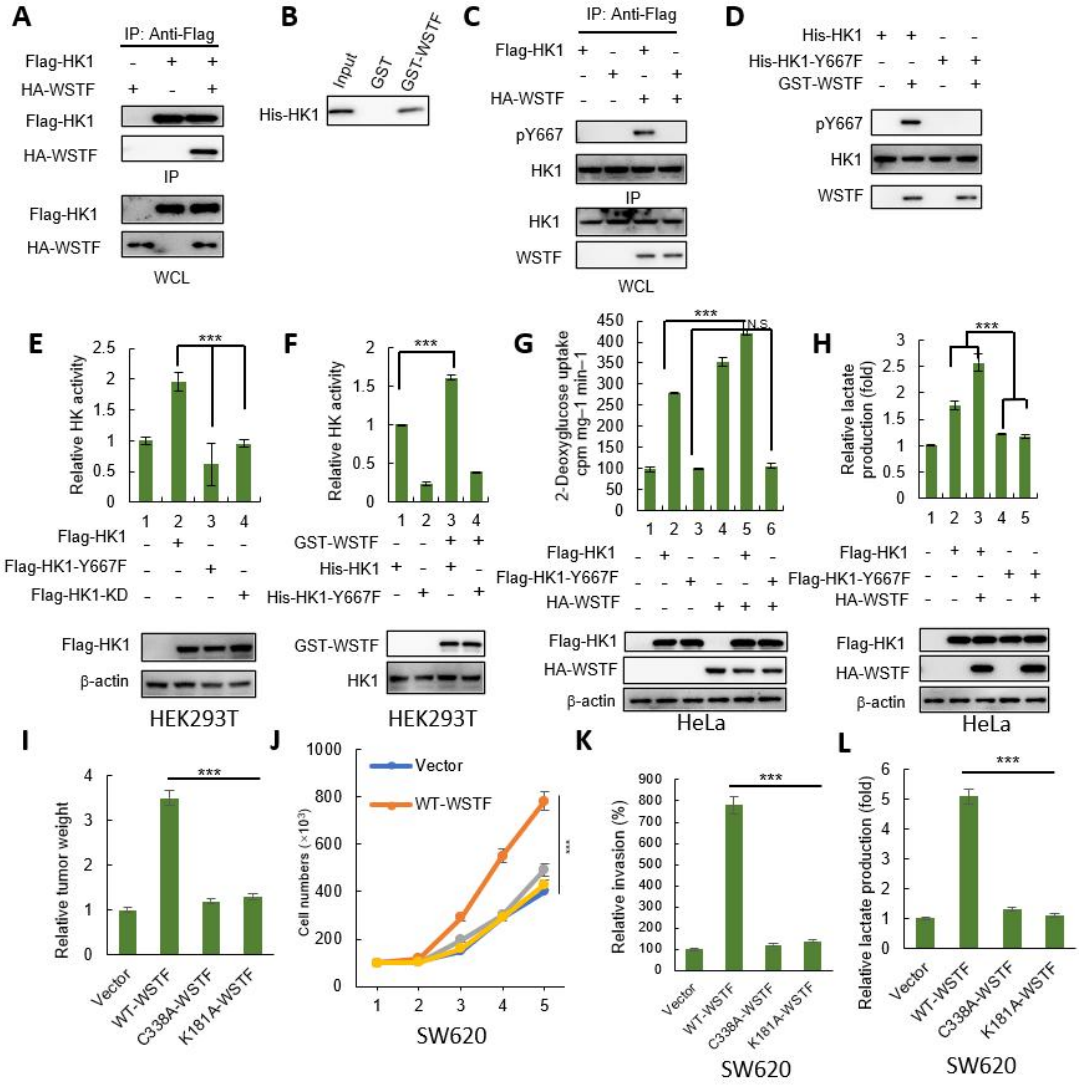

Figure 6. WSTF Directly Binds to and Phosphorylates HK1 to Enhance Its Activity and Promote Tumor Progression-Related Phenotypes

Note: A-B. Co-immunoprecipitation (Co-IP) and GST pull-down assays confirm the physical interaction between WSTF and HK1.

C-D. WSTF directly phosphorylates HK1 at Tyr667, as shown by immunoblotting with a p-Y667-HK1-specific antibody.

E-F. HK1 enzymatic activity is enhanced by WSTF-mediated phosphorylation in HEK293T cells (E) and in vitro (F).

G-H. WSTF increases glucose uptake (G) and lactate production (H) in HeLa cells in a HK1 phosphorylation-dependent manner; this effect is abolished by the HK1-Y667F mutation.

I-L. WT-WSTF, but not the kinase-inactive (C338A) or benzoylation-deficient (K181A) mutants, promotes tumor weight gain in xenografts (I), in vitro cell proliferation (J), Transwell invasion (K), and lactate production (L) in SW620 cells. ***P < 0.001.

4. Discussion

Post-translational modifications (PTMs) and subcellular localization represent core mechanisms governing protein function and are critical drivers of tumor cell proliferation and metabolic reprogramming (Dutta et al., 2023). Williams syndrome transcription factor (WSTF), a well-characterized nuclear protein and histone tyrosine kinase, has long been linked to chromatin remodeling and transcriptional regulation (Lu et al., 1998; Peoples et al., 1998; Barnett & Krebs, 2011; Sharif et al., 2021). In this study, we report that WSTF unexpectedly accumulates in the cytoplasm of multiple cancer cell lines, and that its nucleocytoplasmic shuttling is controlled by a previously unrecognized lysine benzoylation modification at K181. Mechanistically, our data identify GCN5 as the primary benzoyl transferase responsible for WSTF K181 benzoylation, which promotes WSTF nuclear export. Functionally, we demonstrate that cytoplasmic WSTF acts as a non-canonical tyrosine kinase to phosphorylate hexokinase 1 (HK1) at Y667, thereby enhancing HK1 activity, accelerating glycolysis, and promoting tumor growth. Importantly, several key mechanistic links remain inferred rather than directly proven, which should be acknowledged as limitations of the current study.

The most novel finding of this study is the identification of GCN5-mediated benzoylation as a molecular switch controlling WSTF nucleocytoplasmic trafficking. Our data directly demonstrate that GCN5-dependent K181 benzoylation is essential for WSTF nuclear export. However, a critical unresolved question is whether the cytoplasmic pool of WSTF is indeed benzoylated. Although we have shown that K181 benzoylation is required for nuclear export, we have not performed immunoprecipitation of WSTF from fractionated nuclear and cytoplasmic lysates followed by detection with the K181-specific benzoylation antibody, which would provide direct biochemical evidence for cytoplasmic benzoylated WSTF. This important link remains a reasonable inference (Figure 7).

A second key unresolved issue concerns the spatiotemporal coordination of WSTF modification and nuclear export. Our results indicate that GCN5, which catalyzes WSTF benzoylation, is predominantly localized in the nucleus. It remains unclear how nuclear-localized GCN5-mediated benzoylation of WSTF is temporally and spatially coordinated with its subsequent nuclear export, and the precise mechanism that links nuclear benzoylation to cytoplasmic translocation requires further investigation.

Third, although we demonstrate that cytoplasmic WSTF functions via its intrinsic tyrosine kinase activity, whether K181 benzoylation directly regulates or modulates WSTF kinase activity remains undefined. Our current data show that K181 benzoylation controls WSTF localization, but a direct effect of this modification on WSTF catalytic activity has not been examined.

Functionally, we demonstrate that both WSTF benzoylation and kinase activity are required for its oncogenic effects. In vitro and in vivo functional assays confirm that loss of either function

abrogates WSTF-driven proliferation, migration, and glycolysis. Collectively, these findings support a model in which GCN5-mediated WSTF benzoylation promotes nuclear export, enabling cytoplasmic WSTF to phosphorylate HK1 and drive tumor glycolysis.

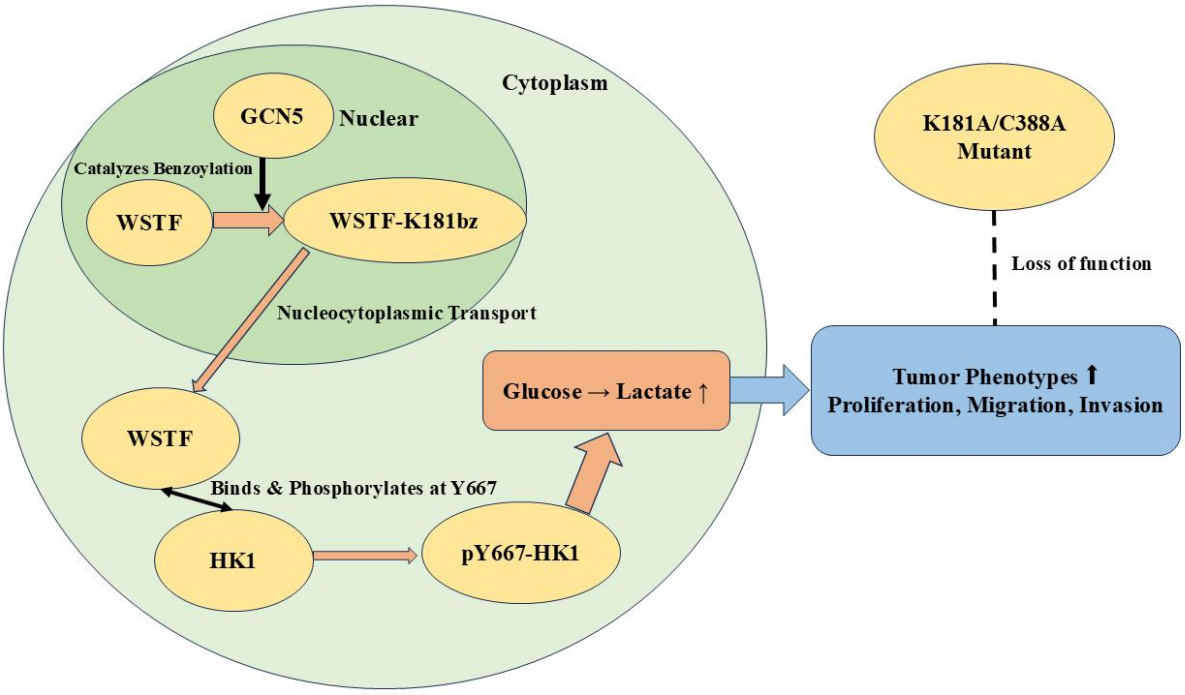

Figure 7.Conversion Path Relationship Diagram

This study has several important limitations that should be acknowledged. First, we lack direct biochemical evidence that the cytoplasmic pool of WSTF carries the K181 benzoylation modification. Immunoprecipitation of WSTF from fractionated nuclear and cytoplasmic lysates followed by K181-benzoylation antibody detection would provide definitive evidence but has not been performed in the current study. Second, the spatiotemporal coordination between nuclear GCN5-mediated WSTF benzoylation and subsequent nuclear export remains unclear. How nuclear modification signals are coupled to cytoplasmic translocation is not yet understood. Third, whether K181 benzoylation directly influences the intrinsic tyrosine kinase activity of WSTF remains uncharacterized. While our data support the proposed regulatory axis, these unresolved questions represent important gaps in the current mechanistic understanding.

In conclusion, this study uncovers a novel regulatory mechanism by which GCN5-catalyzed WSTF benzoylation controls its nucleocytoplasmic shuttling and identifies cytoplasmic WSTF as a non-canonical tyrosine kinase that activates tumor glycolysis via HK1 phosphorylation. GCN5, WSTF K181 benzoylation, and HK1 Y667 phosphorylation represent promising candidate targets for future tumor metabolic intervention strategies, although further validation is required. Addressing the unresolved questions regarding cytoplasmic benzoylated WSTF, spatiotemporal coordination of modification and trafficking, and the potential effect of benzoylation on WSTF kinase activity will be important directions for future investigation.

Author Contributions:

L.Y.W., P.Y.J., W.S.Q., S.Z.H., performed the experiments; W.S.Q. and L.Y. designed most of the experiments; L.Y.W., W.S.Q., Y.L analysed the data and wrote the manuscript. All authors have read and agreed to the published version of the manuscript.

Institutional Review Board Statement:

This study was conducted in strict accordance with the guidelines for animal experiments approved by the Ethics Committee of North China University of Science and Technology. The experimental protocol involving mice was reviewed and formally approved by the above-mentioned Ethics Committee (Approval Number: Q2024020).

The breast cancer and colon cancer cell lines used in this study were commercially purchased and authenticated prior to experiments. All cell culture procedures were performed in compliance with standard laboratory safety and ethical guidelines.

All experimental procedures involving live mice were performed in compliance with the Animal Research: Reporting of In Vivo Experiments (ARRIVE) guidelines and the National Institutes of Health (NIH) Guide for the Care and Use of Laboratory Animals. Every effort was made to minimize the suffering of the animals and reduce the number of animals used.

The authors confirm that all ethical considerations related to this study have been fully addressed, and no potential ethical violations were involved in the entire research process.

All experimental procedures involving live vertebrates were performed in compliance with the Animal Research: Reporting of In Vivo Experiments (ARRIVE) guidelines and were approved by the Animal Ethics Committee of North China University of Science and Technology.

The authors confirm that all ethical considerations related to this study have been fully addressed, and no potential ethical violations were involved in the entire research process.

Informed Consent Statement:

Not applicable.

Data Availability Statement:

The transcriptomic data supporting the findings of this study have been deposited in a public database with the accession number OEP00006795 and are openly accessible. Other raw data, including original Western blot images, have been properly archived and are available from the corresponding authors upon reasonable request. The plasmids constructed in this study (wild-type and mutant WSTF, GCN5, and HK1 expression plasmids) are available free of charge to researchers for non-commercial purposes, subject to a Material Transfer Agreement (MTA).

Acknowledgments:

This work was financially supported by the Central Government Guidance Fund for Local Scientific and Technological Development Projects (Grant No. 246Z7740G), the Talent Funding Project of Tangshan City (Grant No. B202509004), the Science and Technology Plan Project of Tangshan City (Grant No. 25150204E).

Conflict of Interest:

The authors declare no conflict of interest.

References

Addicks, G. C., Zhang, H., Ryu, D., Vasam, G., Green, A. E., Marshall, P. L., et al. (2022). GCN5 maintains muscle integrity by acetylating YY1 to promote dystrophin expression. Journal of Cell Biology, 221(2), e202104022. https://doi.org/10.1083/jcb.202104022

Barnett, C., & Krebs, J. E. (2011). WSTF does it all: A multifunctional protein in transcription, repair, and replication. Biochemistry and Cell Biology, 89(1), 12 – 23. https://doi.org/10.1139/O10-136

Carrillo-Rosas, S., Weber, C., Fievet, L., Messaddeq, N., Karam, A., & Trottier, Y. (2019). Loss of zebrafish Ataxin-7, a SAGA subunit responsible for SCA7 retinopathy, causes ocular coloboma and malformation of photoreceptors. Human Molecular Genetics, 28(6), 912–927. https://doi.org/10.1093/hmg/ddy401

Chen, L., Wei, T., Si, X., Wang, Q., Li, Y., Leng, Y., et al. (2013). Lysine acetyltransferase GCN5 potentiates the growth of non-small cell lung cancer via promotion of E2F1, cyclin D1, and cyclin E1 expression. Journal of Biological Chemistry, 288(20), 14510 – 14521. https://doi.org/10.1074/jbc.M112.415266

Dutta, H., & Jain, N. (2023). Post-translational modifications and their implications in cancer. Frontiers in Oncology, 13, 1240115. https://doi.org/10.3389/fonc.2023.1240115

Farria, A. T., Plummer, J. B., Salinger, A. P., Shen, J., Lin, K., Lu, Y., et al. (2020). Transcriptional activation of MYC-induced genes by GCN5 promotes B-cell lymphomagenesis. Cancer Research, 80(24), 5543 – 5553. https://doi.org/10.1158/0008-5472.CAN-20-1240

Hanahan, D., & Weinberg, R. A. (2011). Hallmarks of cancer: The next generation. Cell, 144(5), 646–674. https://doi.org/10.1016/j.cell.2011.02.013

Hennig, E. E., Mikula, M., Rubel, T., Dadlez, M., & Ostrowski, J. (2012). Comparative kinome analysis to identify putative colon tumor biomarkers. Journal of Molecular Medicine, 90(4), 447–456. https://doi.org/10.1007/s00109-011-0827-7

Huang, H., Fu, Y., Duan, Y., Zhang, Y., Lu, M., Chen, Z., et al. (2022). Suberoylanilide hydroxamic acid (SAHA) treatment reveals crosstalk among proteome, phosphoproteome, and acetylome in nasopharyngeal carcinoma cells. Frontiers in Genetics, 13, 873840. https://doi.org/10.3389/fgene.2022.873840

Kahl, M., Brioli, A., Bens, M., Perner, F., Kresinsky, A., Schnetzke, U., et al. (2019). The acetyltransferase GCN5 maintains ATRA-resistance in non-APL AML. Leukemia, 33(11), 2628–2639. https://doi.org/10.1038/s41375-019-0480-4

Kang, D., Liu, Y., Song, Y., Fang, B., Zhang, Q., & Hu, L. (2022). Triptolide shows high sensitivity and low toxicity against acute myeloid leukemia cell lines through inhibiting WSTF-RNAPII complex. Frontiers in Oncology, 12, 811850. https://doi.org/10.3389/fonc.2022.811850

Kierans, S. J., & Taylor, C. T. (2024). Glycolysis: A multifaceted metabolic pathway and signaling hub. Journal of Biological Chemistry, 300(11), 107906. https://doi.org/10.1016/j.jbc.2024.107906

Koutsogiannouli, E. A., Wagner, N., Hader, C., Pinkerneil, M., Hoffmann, M. J., & Schulz, W. A. (2017). Differential effects of histone acetyltransferase GCN5 or PCAF knockdown on urothelial carcinoma cells. International Journal of Molecular Sciences, 18(7), 1443. https://doi.org/10.3390/ijms18071443

Kumar, A., Bhowmick, K., Vikramdeo, K. S., Mondal, N., Subbarao, N., & Dhar, S. K. (2017). Designing novel inhibitors against histone acetyltransferase (HAT: GCN5) of Plasmodium falciparum. European Journal of Medicinal Chemistry, 138, 26 – 37. https://doi.org/10.1016/j.ejmech.2017.06.027

Lerin, C., Rodgers, J. T., Kalume, D. E., Kim, S. H., Pandey, A., & Puigserver, P. (2006). GCN5 acetyltransferase complex controls glucose metabolism through transcriptional repression of PGC-1α. Cell Metabolism, 3(6), 429–438. https://doi.org/10.1016/j.cmet.2006.04.013

Leung, Y. T., Shi, L., Maurer, K., Song, L., Zhang, Z., Petri, M., et al. (2015). Interferon regulatory factor 1 and histone H4 acetylation in systemic lupus erythematosus. Epigenetics, 10(3), 191–199. https://doi.org/10.1080/15592294.2015.1017197

Li, B., Sun, J., Dong, Z., Xue, P., He, X., Liao, L., et al. (2016). GCN5 modulates osteogenic differentiation of periodontal ligament stem cells through DKK1 acetylation in inflammatory microenvironment. Scientific Reports, 6, 26542. https://doi.org/10.1038/srep26542

Li, J., Xiang, L., Wang, S., Zhang, Y., Zhao, S., Zhang, D., et al. (2025). Targeting the crosstalk between glutamine metabolism and tumor immune microenvironment for lung cancer immunotherapy. Interdisciplinary Medicine, 3(2), e20240069. https://doi.org/10.1002/inmd.20240069

Li, J., Yan, C., Wang, Y., Chen, C., Yu, H., Liu, D., et al. (2022). GCN5-mediated regulation of pathological cardiac hypertrophy via activation of the TAK1-JNK/p38 signaling pathway. Cell Death & Disease, 13(4), 421. https://doi.org/10.1038/s41419-022-04863-5

Li, Y., Liu, Y., Deng, Y., Wang, S., Song, M., Chen, S., et al. (2016). Regulation of H3K9ac and H4K16ac by the PCAF/WSTF/MOF complex in breast cancer cells. Genomics and Applied Biology, 35(5), 1008–1012.

Liu, K., Zhang, Q., Lan, H., Wang, L., Mou, P., Shao, W., et al. (2015). GCN5 potentiates glioma proliferation and invasion via STAT3 and AKT signaling pathways. International Journal of Molecular Sciences, 16(9), 21897–21910. https://doi.org/10.3390/ijms160921897

Liu, Y., Wang, S. Q., Long, Y. H., Chen, S., Li, Y. F., & Zhang, J. H. (2016). KRASG12 mutant induces the release of the WSTF/NRG3 complex, and contributes to an oncogenic paracrine signaling pathway. Oncotarget, 7(33), 53153 – 53164. https://doi.org/10.18632/oncotarget.10803

Liu, Y., Zhang, Y. Y., Wang, S. Q., Li, M., Long, Y. H., Li, Y. F., et al. (2020). WSTF acetylation by MOF promotes WSTF activities and oncogenic functions. Oncogene, 39(27), 5056–5067. https://doi.org/10.1038/s41388-020-1325-8

Lu, X., Meng, X., Morris, C. A., & Keating, M. T. (1998). A novel human gene, WSTF, is deleted in Williams syndrome. Genomics, 54(2), 241 – 249. https://doi.org/10.1006/geno.1998.5570

Majaz, S., Tong, Z., Peng, K., Wang, W., Ren, W., Li, M., et al. (2016). Histone acetyl transferase GCN5 promotes human hepatocellular carcinoma progression by enhancing AIB1 expression. Cell & Bioscience, 6, 47. https://doi.org/10.1186/s13578-016-0113-x

Mao, X., Gluck, N., Li, D., Maine, G. N., Li, H., Zaidi, I. W., et al. (2009). GCN5 is a required cofactor for a ubiquitin ligase that targets NF-kappaB/RelA. Genes & Development, 23(7), 849–861. https://doi.org/10.1101/gad.1748409

Meng, J., Zhang, X. T., Liu, X. L., Fan, L., Li, C., Sun, Y., et al. (2016). WSTF promotes proliferation and invasion of lung cancer cells by inducing EMT via PI3K/Akt and IL-6/STAT3 signaling pathways. Cellular Signalling, 28(11), 1673 – 1682. https://doi.org/10.1016/j.cellsig.2016.08.005

Nargund, A. M., Xu, C., Mandoli, A., Okabe, A., Chen, G. B., Huang, K. K., et al. (2022). Chromatin rewiring by mismatch repair protein MSH2 alters cell adhesion pathways and sensitivity to BET inhibition in gastric cancer. Cancer Research, 82(14), 2538 – 2551. https://doi.org/10.1158/0008-5472.CAN-21-3642

Oh, J. H., Lee, J. Y., Kim, K. H., Kim, C. Y., Jeong, D. S., Cho, Y., et al. (2020). Elevated GCN5 expression confers tamoxifen resistance by upregulating AIB1 expression in ER-positive breast cancer. Cancer Letters, 495, 145–155. https://doi.org/10.1016/j.canlet.2020.09.019

Peoples, R. J., Cisco, M. J., Kaplan, P., & Francke, U. (1998). Identification of the WBSCR9 gene, encoding a novel transcriptional regulator, in the Williams-Beuren syndrome deletion at 7q11.23. Cytogenetics and Cell Genetics, 82(3 – 4), 238 – 246. https://doi.org/10.1159/000015099

Qiao, L., Zhang, Q., Zhang, W., & Chen, J. J. (2018). The lysine acetyltransferase GCN5 contributes to human papillomavirus oncoprotein E7-induced cell proliferation via up-regulating E2F1. Journal of Cellular and Molecular Medicine, 22(11), 5333 – 5345. https://doi.org/10.1111/jcmm.13793

Ren, X., Zhou, Y., Xue, Z., Hao, N., Li, Y., Guo, X., et al. (2021). Histone benzoylation serves as an epigenetic mark for DPF and YEATS family proteins. Nucleic Acids Research, 49(1), 114–126. https://doi.org/10.1093/nar/gkaa1115

Shao, G., Liu, Y., Ma, T., Zhang, L., Yuan, M., & Zhao, S. (2018). GCN5 inhibition prevents IL-6-induced prostate cancer metastases through PI3K/PTEN/Akt signaling by inactivating Egr-1. Bioscience Reports, 38(6), BSR20180714. https://doi.org/10.1042/BSR20180714

Sharif, S. B., Zamani, N., & Chadwick, B. P. (2021). BAZ1B the protean protein. Genes, 12(10), 1541. https://doi.org/10.3390/genes12101541

Smith, T. A. (2000). Mammalian hexokinases and their abnormal expression in cancer. British Journal of Biomedical Science, 57(2), 170–178.

Wang, Y. Q., Liu, Y., Li, Y. F., Zhang, J. H., Liu, Y., Li, Y., et al. (2016). Williams syndrome transcription factor is a target of pro-oncogenic Ser158 phosphorylation mediated by Ras-MAPK pathway in human breast cancer. In Proceedings/Conference abstracts.

Wilson, J. E. (2003). Isozymes of mammalian hexokinase: Structure, subcellular localization and metabolic function. Journal of Experimental Biology, 206(Pt 12), 2049 – 2057. https://doi.org/10.1242/jeb.00241

Yin, Y. W., Jin, H. J., Zhao, W., Gao, B., Fang, J., Wei, J., et al. (2015). The histone acetyltransferase GCN5 expression is elevated and regulated by c-Myc and E2F1 transcription factors in human colon cancer. Gene Expression, 16(4), 187 – 196. https://doi.org/10.3727/105221615X14399878166161

Yuan, Y., Liu, J., Yu, X., Liu, X., Cheng, Y., Zhou, C., et al. (2021). Tumor-targeting pH/redox dual-responsive nanosystem epigenetically reverses cancer drug resistance by co-delivering doxorubicin and GCN5 siRNA. Acta Biomaterialia, 135, 556 – 566. https://doi.org/10.1016/j.actbio.2021.08.042

Zhang, Y. J., Lu, C. R., Cao, Y., Luo, Y., Bao, R. F., Yan, S., et al. (2012). Imatinib induces H2AX phosphorylation and apoptosis in chronic myelogenous leukemia cells in vitro via caspase-3/Mst1 pathway. Acta Pharmacologica Sinica, 33(4), 551 – 557. https://doi.org/10.1038/aps.2011.192